Polarity-dependent charge density wave in the kagome superconductor CsV$_3$Sb$_5$

Takemi Kato [1,*] Yongkai Li,[2,3,4,*] Kosuke Nakayama [1,5,†] Zhiwei Wang [2,3,4,‡] Seigo Souma,[6,7] Miho Kitamura,[8]
Koji Horiba,[8,9] Hiroshi Kumigashira [10] Takashi Takahashi,[1,7] and Takafumi Sato[1,6,7,11,§]

[1]*Department of Physics, Graduate School of Science, Tohoku University, Sendai 980-8578, Japan*
[2]*Centre for Quantum Physics, Key Laboratory of Advanced Optoelectronic Quantum Architecture and Measurement (MOE),*
School of Physics, Beijing Institute of Technology, Beijing 100081, People's Republic of China
[3]*Beijing Key Laboratory of Nanophotonics and Ultrafine Optoelectronic Systems, Beijing Institute of Technology,*
Beijing 100081, People's Republic of China
[4]*Material Science Center, Yangtze Delta Region Academy of Beijing Institute of Technology, Jiaxing 314011,*
People's Republic of China
[5]*Precursory Research for Embryonic Science and Technology (PRESTO), Japan Science and Technology Agency (JST),*
Tokyo 102-0076, Japan
[6]*Center for Spintronics Research Network, Tohoku University, Sendai 980-8577, Japan*
[7]*Advanced Institute for Materials Research (WPI-AIMR), Tohoku University, Sendai 980-8577, Japan*
[8]*Institute of Materials Structure Science, High Energy Accelerator Research Organization (KEK), Tsukuba, Ibaraki 305-0801, Japan*
[9]*National Institutes for Quantum Science and Technology (QST), Sendai 980-8579, Japan*
[10]*Institute of Multidisciplinary Research for Advanced Materials (IMRAM), Tohoku University, Sendai 980-8577, Japan*
[11]*International Center for Synchrotron Radiation Innovation Smart (SRIS), Tohoku University, Sendai 980-8577, Japan*

Polar surface and interface play pivotal roles for realizing exotic properties of materials, and search for such polar states is of crucial importance for expanding materials' functionality. Here we report microfocused angle-resolved photoemission spectroscopy of CsV$_3$Sb$_5$, a member of recently discovered kagome superconductors AV$_3$Sb$_5$ (A = K, Rb, and Cs) and show evidence for the polar nature of the cleaved surface which is characterized by Cs- and Sb-terminated surfaces with markedly different fermiology. The Cs-terminated surface shows intriguing doubling of V-derived bands at low temperatures associated with the band folding due to the three-dimensional charge density wave (CDW), whereas the Sb-terminated one shows no band doubling or resultant CDW-gap opening indicative of the suppression of bulk-originated CDW due to polar charge. Such polar-surface-dependent band structures must be incorporated for understanding the origin of unconventional superconducting and charge order at the surface of AV$_3$Sb$_5$.

The surface and interface of crystals are a fertile playground where a variety of exotic properties emerge owing to its symmetry, chemical bonding, and topological characteristics distinct from those of a bulk counterpart. A sudden change in the electrostatic potential at the surface generates conducting two-dimensional (2D) electron gas called Shockley states [1] which evolve into spin-split Rashba states associated with the space-inversion symmetry breaking [2], whereas the discontinuity of the topological index across the surface of topological insulators leads to spin-helical Dirac-cone states [3–5]. Another key factor that gives a significant influence on physical properties at the surface/interface is polarity; its impact is best demonstrated at the interface of ionic crystals where the electronic band structure is markedly reconstructed so as to compensate the discontinuity of ionic

polarity (known as polar catastrophe). For instance, the LaAlO$_3$/SrTiO$_3$ interface exhibits high conductivity and even superconductivity despite the semiconducting nature of host crystals [6–8]. Polarity also plays an essential role at polar surfaces to bring about various exotic properties as represented by Rashba-split 2D electron gas at SrTiO$_3$ surface [9–12], extremely overdoped CuO$_2$ planes at a high-temperature superconductor YBa$_2$Cu$_3$O$_7$ surface [13,14], a ferromagnetic surface of antiferromagntic PdCoO$_2$ [15], spin-texture manipulation in giant Rashba compound BiTeI [16,17], and surface-termination-dependent Fermi arcs in Weyl semimetal NbP [18]. As highlighted by these examples, understanding the physics associated with the polar surfaces of quantum materials is a key topic of modern condensed-matter physics.

Here we focus on CsV$_3$Sb$_5$, a member of kagome metals AV$_3$Sb$_5$ (A = K, Rb, and Cs) which were recently discovered to show superconductivity with T_c = 0.9–2.5 K coexisting with charge density wave (CDW) below T_{CDW} = 78–103 K [19–21] with the in-plane 2×2 periodicity [22–29]. The crystal structure of CsV$_3$Sb$_5$ consists of two building blocks,

_____

*These authors contributed equally to this work.
†k.nakayama@arpes.phys.tohoku.ac.jp
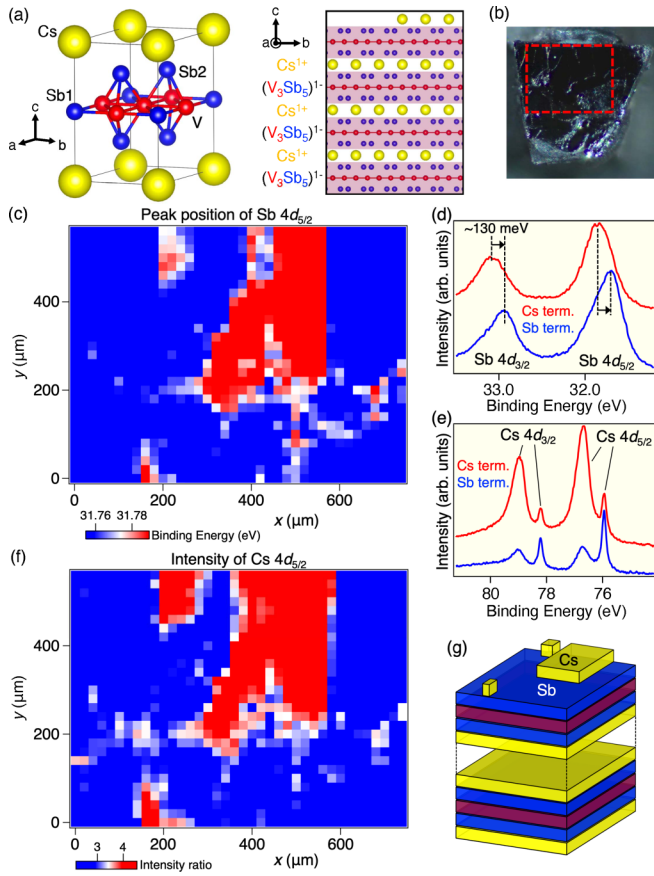‡zhiweiwang@bit.edu.cn
§t-sato@arpes.phys.tohoku.ac.jp

FIG. 1. (a) Crystal structure of CsV_3Sb_5. (b) Photograph of a cleaved CsV_3Sb_5 single crystal. (c) Spatial map of the E_B position of Sb-4$d_{5/2}$ core level measured with $h\nu = 106$ eV at $T = 8$ K in the spatial region enclosed by red dashed rectangle (area size: $600 \times 800 \, \mu m^2$) in (b), obtained with the step size of 20 μm. (d) and (e) EDC in the Sb-4d and Cs-4d core-level regions, respectively, for the Cs-(red) and Sb-(blue) terminated surfaces. (f) Spatial map of the intensity ratio of the surface/bulk Cs-4$d_{5/2}$ core-level peaks. (g) Schematic of the cleaved surface of CsV_3Sb_5.

a Cs layer, and a V_3Sb_5 layer, and the cleaved surface is expected to be terminated either by the Cs or V_3Sb_5 (Sb2) layer [Fig. 1(a)]. Although the bonding between V and Sb1/Sb2 atoms within the V_3Sb_5 layer may be intermetallic, the coupling between the Cs and V_3Sb_5 layers is ionic because Cs is fully ionized (Cs^{1+}) to donate one electron to the V_3Sb_5 layer [$(V_3Sb_5)^{1-}$]. Such ionicity would lead to polar instability. In fact, two different surface terminations have been identified by scanning-tunneling-microscopy (STM) measurements, and intriguingly, there is growing experimental evidence that such a surface hosts peculiar quantum states distinct from those of the bulk as exemplified by the formation of unidirectional 4×1 CDW [22,24–30], surface-dependent vortex-core states [25], and the pair-density wave [22]. However, the band structure associated with the polar surface remains totally unexplored in AV_3Sb_5.

In this Letter, we report a spatially resolved angle-resolved photoemission spectroscopy (ARPES) study of CsV_3Sb_5. By utilizing the microfocused photon beam from the synchrotron, we have succeeded in separately observing two kinds of po-

lar surfaces and uncovered marked differences in the band structures between them. The Cs-terminated surface shows the band doubling associated with the three-dimensional (3D) nature of CDW at low temperatures, whereas the Sb-terminated surface is strongly hole doped, resulting in the suppression of CDW. We discuss implications of the present results in relation to the mechanism of the CDW and unconventional surface properties.

High-quality CsV_3Sb_5 single crystals were synthesized with the self-flux method [31]. ARPES measurements were performed using Scienta-Omicron DA30 and SES2002 spectrometers at BL-28A and BL-2A in Photon Factory, KEK. We used energy tunable photons of $h\nu = 85$–350 eV. ARPES data were mainly obtained by circularly polarized 106-eV photons (corresponding to the out-of-plane wave vector $k_z \sim 0$) [32] with the beam spot size of $10 \times 12 \, \mu m^2$ [33]. The energy resolution was set to be 25 meV. The samples were cleaved at the same temperatures at which the ARPES measurements were performed (8 and 120 K). All the data have been recorded within 8 hs after the cleavage. Within this time period, we did not observe discernible shifts in band energy. Thus, the doping effect discussed later is not related to the time-dependent doping effect reported earlier [34].

First, we demonstrate how to distinguish two types of polar surfaces. The cleaved surface of CsV_3Sb_5 contains a flat shiny mirrorlike region [Fig. 1(b)]. By sweeping the microfocused photon beam on the surface, we have mapped out the spatial distribution of the binding energy (E_B) of Sb-4$d_{5/2}$ core-level peak [see Fig. 1(c)], which is a good measure of the surface doping level (note that the selection of the Sb-4$d_{3/2}$ peak reproduces the same result). As seen in Fig. 1(c), the surface looks to consist of two regions (blue and red regions). The core-level spectrum in the red region [red curve in Fig. 1(d)] is shifted as a whole toward higher E_B by ~ 130 meV with respect to that in the blue region (blue curve), indicating that the red region is more electron doped than the blue region (see Sec. 1 of the Supplemental Material for detailed discussion on the origin of the Sb-4d core-level shift [35]). Such a difference in the doping level signifies different polarities of the two regions. Here we assign the electron (hole)-rich red (blue) region to the Cs (Sb)-terminated surface because Cs atoms on top surface do not need to donate electrons to the missing upper V_3Sb_5 layer which is removed by the cleaving so that the V_3Sb_5 layer beneath the topmost Cs layer is more electron doped for the Cs-terminated surface. Inversely, the V_3Sb_5 layer at the surface is hole doped compared with the bulk counterpart. This is also corroborated by the behavior of the Cs-4d core level. Figure 1(e) shows the Cs-4d core-level spectra measured at the same spatial location as in Fig. 1(d) where we observe that each spin-orbit satellite of Cs-4d core levels ($d_{5/2}$ or $d_{3/2}$) consists of two peaks; a peak at lower E_B originates from bulk Cs atoms whereas that at higher E_B is from surface Cs atoms as confirmed by the angular dependence of their intensity ratio (Sec. 1 of the Supplemental Material [35]). One can recognize that the surface Cs peak is stronger than the bulk one for the Cs-termination-dominant surface (red curve), whereas it is weaker for the Sb-termination-dominant case (blue curve) (see Sec. 2 of the Supplemental Material for the analysis of peak position [35]). The spatial image of the intensity ratio between the surface and the bulk Cs peaks in
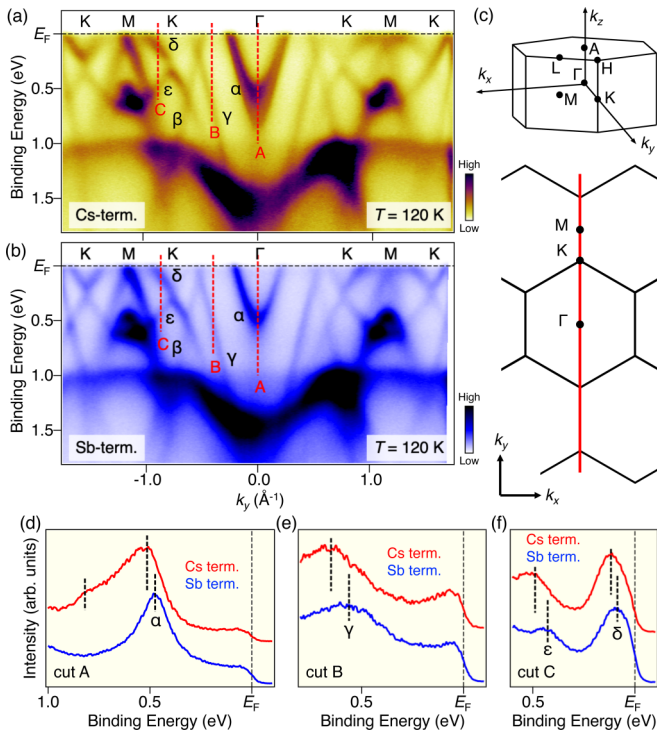
FIG. 2. (a) and (b) ARPES intensity at $T = 120$ K for Cs- and Sb-terminated surfaces, respectively, measured with $h\nu = 106$ eV along the ΓKM cut. (c) (top) Bulk Brillouin zone and (bottom) slice of the Brillouin zone at $k_z = 0$ plane. (d)–(f) Comparison of the EDCs measured for the Cs (red) and Sb (blue) surface terminations at **k** cuts A–C, respectively. The position of **k** cuts is indicated by red dashed lines in (a) and (b).

Fig. 1(f) shows good agreement with that of the Sb-core-level E_B in Fig. 1(c). This supports our assignment of the Cs- and Sb-termination-dominant surfaces (hereafter, we simply call them Cs- and Sb-terminated surfaces, respectively) as schematically shown in Fig. 1(g).

We show in Figs. 2(a) and 2(b) the ARPES intensity at $T = 120$ K (above $T_{CDW} = 93$ K) along the ΓKM cut ($k_z \sim 0$) [red line in Fig. 2(c)] for the Cs- and Sb-terminated surfaces, respectively. One can recognize overall similarity in the band structure between the two, i.e., an electron band at the Γ point (α) with the Sb-5p_z character, linearly dispersive V-3$d_{xz/yz}$ bands (β, γ) forming a Dirac cone near E_F (marked by an arrow), the δ band with the V-3d_{xy/x^2-y^2} character forming a saddle point (SP) slightly above E_F, and the ε band that intersects the δ band to form a Dirac point at the K point at $E_B \sim 0.3$ eV [23,24,32,36–39]. A closer look further reveals some intrinsic differences; the band structure of the Cs-terminated surface is shifted downward as a whole with respect to that of the Sb-terminated surface as recognized by a direct comparison of surface-termination-dependent ARPES spectra at representative **k** points plotted in Figs. 2(d)–2(f) in which numerical fittings to the peak position clarified the energy shift to be 30–90 meV (note that a finite variation in the magnitude of the energy shift among different bands and Sb-4d core levels suggests a non-rigid-band-type energy shift; also see Sec. 3 of the Supplemental Material for the energy shift of the δ band [35]). Moreover, whereas the

Sb-terminated surface exhibits a single α band bottomed at $E_B \sim 0.5$ eV, it splits into two bands bottomed at $E_B \sim 0.5$ and 0.8 eV for the Cs-terminated surface. This suggests that not only polarity, but also the band structure above T_{CDW} is different between the Cs- and the Sb-terminated surfaces. We have performed ARPES measurements more than three times with different samples for each surface termination and confirmed the reproducibility (see Sec. 4 of the Supplemental Material [35]).

Next we analyze the electronic structure of the Cs-terminated surface in more detail, particularly, in relation to the CDW transition. Figures 3(a) and 3(b) show a comparison of the Fermi-surface (FS) mapping at the $k_z \sim 0$ plane between $T = 120$ (above T_{CDW}) and 8 K (below T_{CDW}). At $T = 120$ K, one can recognize a small circular and a large hexagonal pocket centered at the Γ point together with a triangular pocket at the K point [32,40–47]. On the other hand, at $T = 8$ K, the hexagonal pocket splits into two pockets as more clearly seen in Figs. 3(c) and 3(d) where the enlarged FS image is displayed. Such a band splitting is observed in a wide $(E, \mathbf{k})$ region as highlighted by the ARPES intensity at $T = 8$ K measured along the representative k_y cuts at $k_x = 0$ and $-\pi$ in Figs. 3(e) and 3(f). For example, the δ and the ε bands show an energy splitting as better visualized in Fig. 3(e) [also see the energy distribution curve (EDC) in Sec. 5 of the Supplemental Material [35]]. Also, the β and γ bands show splitting as seen in Fig. 3(f) [note that there are two peaks in the momentum distribution curve [(MDC); red curves] in the Supplemental Material [35]] and in the corresponding second-derivative intensity in Fig. 3(g). Thus, in the CDW phase, all the V-derived bands show splitting. It is noted, however, that although the Sb-derived α band appears to split, it is unclear whether it is of the CDW origin because the splitting was also observed at $T = 120$ K [Fig. 2(a)]. The origin of the α-band splitting in the normal state has been discussed in connection with the formation of quantum well states [48] and the k_z broadening effect [32].

Now, we discuss the origin of the band splitting for the V-derived bands. Apparently, it is not associated with the exchange splitting because no signature of ferromagnetism was reported in AV$_3$Sb$_5$ [31]. The existence of surface states near the main bulk bands and the influence of the k_z broadening would be also unlikely, because the splitting is absent at $T = 120$ K. A plausible explanation is the CDW-potential-induced band folding along the k_z direction, which is naturally expected from the reported 3D nature of CDW accompanied by the out-of-plane unit-cell doubling ($2 \times 2 \times 2$) [25,40] (see Fig. S8 in the Supplemental Material for details [35]). It is noted that we also found a signature of the in-plane band folding as detailed in Sec. 6 of the Supplemental Material [35].

We measured the δ-band dispersion along the MK cut which forms the SP at $T = 8$ K [Fig. 3(h)] and revealed that it disperses back toward higher E_B without reaching E_F due to the CDW-gap opening. This gap is well seen from the EDC at the Fermi wave vector (k_F) [indicated by triangle in Fig. 3(h)] at $T = 8$ K where a characteristic hump structure appears at $E_B \sim 70$ meV in agreement with previous studies [32,42]. Besides the 70-meV hump, the EDC at $T = 8$ K shows a small peak at $E_B \sim 20$ meV, which may be due to
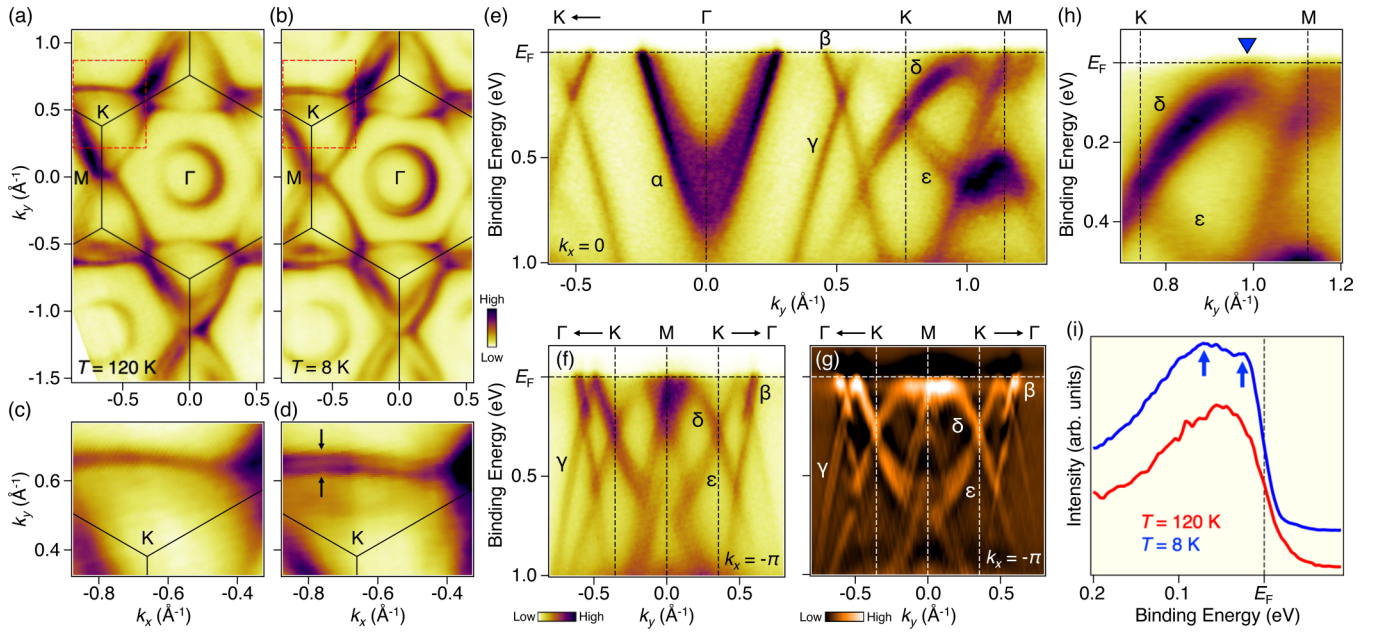
FIG. 3. (a) and (b) FS map for the Cs-terminated surface measured at $T = 120$ K and 8 K, respectively. (c) and (d) Enlarged view in the **k** region enclosed by dashed red rectangle in (a) and (b), respectively. (e) and (f) ARPES intensity plots at $T = 8$ K measured along k_y at $k_x = 0$ (ΓKM cut) and $-\pi$ (KMK cut), respectively. (g) Second-derivative intensity of (f). (h) Plot of near-E_F ARPES intensity at $T = 8$ K along the MK cut obtained with higher resolution. (i) EDCs at $T = 120$ K (red) and 8 K (blue) at the k_F point along the MK cut [blue triangle in (h)]. The hump and peak structures at $T = 8$ K are indicated by blue arrows.

the CDW-gap opening in the folded band from the $k_z = \pi$ plane.

Having established the electronic states of the Cs-terminated surface, now we turn our attention to the Sb-terminated surface. Figure 4(a) shows the typical FS mapping for the Sb-terminated surface at $T = 8$ K well below T_{CDW}. By comparing with that of the Cs-terminated counterpart [Fig. 3(b)], we observe shrinkage of the circular pocket centered at the Γ point and the triangular pocket at the K point due to the excess hole doping in the Sb-terminated surface (see Sec. 7 of the Supplemental Material [35] for quantitative comparison). All the energy bands observed in this Letter have a surface character (specifically, the energy bands of the topmost V$_3$Sb$_5$ layer) because of a relatively short escape depth of photoelectrons (~10 Å). For the Sb-terminated surface, the hole-doped character of the Γ-centered pocket derived from the Sb1 atoms suggests that the hole-doping effect extends to the Sb1-V plane. Taking into account these points, it is natural to observe an energy shift of the V-derived bands. It is noted that, besides the polarity-induced charge doping, the inversion symmetry is broken at the Sb-terminated surface. But the band splitting, e.g., Rashba-type spin splitting, expected by the inversion-symmetry breaking has not been observed within our experimental uncertainty, suggesting that such an effect may not be strong in CsV$_3$Sb$_5$.

More importantly, the band dispersion is basically temperature independent as seen from the ARPES intensity at $T = 8$ K in Fig. 4(b) which is similar to that at $T = 120$ K [Fig. 2(b)]; one can see no doubling of the Sb- and V-derived bands. The absence of band doubling for the Sb-terminated surface is more clearly visualized in Figs. 4(c) and 4(d) where the representative MDCs and EDCs are compared between

the Cs- and the Sb-terminated surfaces (red and blue curves, respectively). We also found that the Sb-terminated surface shows no clear CDW-gap opening. As shown in Fig. 4(e), the δ band simply crosses E_F (see the triangle) without bending back behavior, in contrast to the case of the Cs-terminated surface [see the band dispersion extracted from the peak position of EDCs in Fig. 4(f)]. Also, the EDC at the k_F point for the Sb-terminated surface [blue curve in Fig. 4(g)] exhibits no hump structure unlike the case of the Cs-terminated counterpart (red curve).

The band diagram as a function of surface Cs coverage derived from the present Letter and our previous work on Cs-dosed CsV$_3$Sb$_5$ [36] is summarized in Fig. 5. The excess hole doping realized in the Sb-terminated surface pushes up the energy bands, whereas the electron doping in the Cs-terminated or Cs-dosed surfaces pushes down (note that E_F for the bulk band structure would be obtained by averaging E_F of the Cs and Sb terminations because the electron concentration identical to the bulk is realized at the Cs coverage of 50%). Despite the surface character of observed band structures in the present Letter, a signature of 2×2×2 CDW is found in the Cs-terminated surface at low temperatures, suggesting that the 2×2×2 CDW and the resultant band folding along k_z can survive even at the surface under a certain condition. On the other hand, the 2×2×2 CDW is suppressed in the Sb-terminated and heavily Cs-dosed surfaces. Understanding the relationship between this contrasting CDW behavior and the difference in surface charge is a next important step toward clarifying the mechanism of unconventional CDW in CsV$_3$Sb$_5$.

We discuss implications of the present results in relation to the exotic surface properties recently reported by STM of AV$_3$Sb$_5$ [22,24–29]. One of the intriguing surface properties is
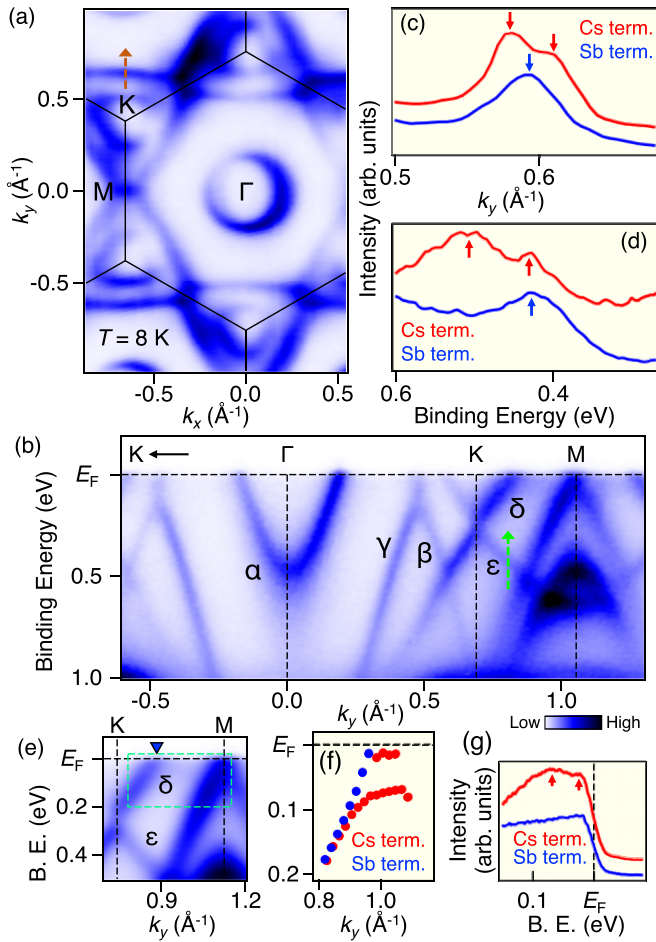
FIG. 4. (a) FS map for the Sb-terminated surface measured at $T = 8$ K with $h\nu = 106$ eV. (b) ARPES-intensity plot at $T = 8$ K measured along the ΓKM cut. (c) Comparison of the MDCs between the Sb- and Cs-terminated surfaces, obtained along the **k** cut indicated by brown dashed arrow in (a). (d) Comparison of EDC between the two surface terminations, obtained in the E_B region shown by dashed green arrow in (b). Arrows in (c) and (d) indicate peak positions of the MDC/EDC. (e) Plot of near-E_F ARPES intensity for the Sb-terminated surface, measured along the MK cut with higher energy resolution at $T = 8$ K. (f) Comparison of experimental band dispersions between the Sb- and Cs-terminated surfaces in the $(E, \mathbf{k})$ region enclosed by dashed green rectangle in (e). (g) Comparison of EDC at the k_F point of the δ band [blue triangle in (e)]. Red arrows show hump-and-peak structure associated with the CDW gap for the Cs-terminated surface.

that the superconducting-gap structure shows a higher density of states at E_F for the Cs-terminated surface compared to the Sb-terminated one [22]. This could be interpreted in terms of the enhanced gap anisotropy in the Cs-terminated surface. In light of our observations, such a difference is suggested to be related to the strength of CDW at the surface; namely, the Cs-terminated surface is more strongly perturbed by CDW so that the superconducting-gap structure becomes more complex and unconventional. Another exotic surface property is the emergence of surface charge order with a unidirectional 4×1 periodicity that appears only for the Sb-terminated surface [22,24–29]. This surface charge order may be associated
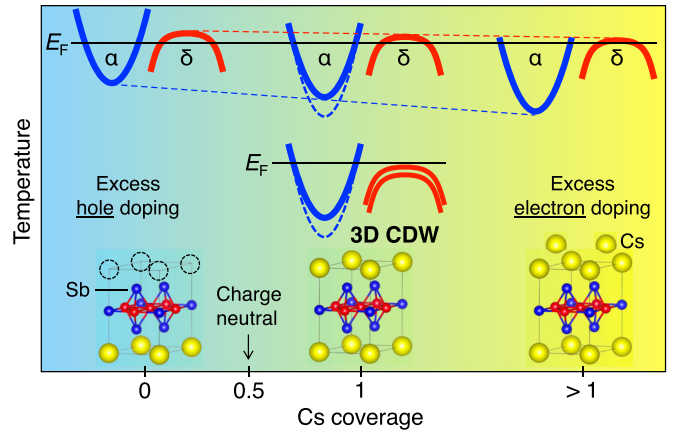

FIG. 5. Schematic of key band structure in CsV$_3$Sb$_5$ as a function of surface Cs coverage. Inset shows the crystal structure at the surface of Sb-terminated (left), Cs-terminated (middle), and Cs-dosed CsV$_3$Sb$_5$ (right).

with the suppression of the 2×2 CDW in light of the present ARPES result (in fact, one may see a finite change in the intensity of 2×2 superspots in the Fourier transform image of the STM pattern [25]). Also, the mechanism of the 4×1 charge order cannot be easily explained from the observed FS topology; it is hard to infer from the FS mapping in Figs. 3(b) and 4(a) that the Sb-terminated surface possesses a good nesting condition with the 4×1 periodicity. This suggests that other possibilities beyond the simple FS nesting, such as electron correlation and surface instability [22,24,26] must be taken into account to understand the unconventional surface charge order; we leave this issue as an open question. In any case, the present Letter strongly suggests that the polarity-dependent band characteristics, such as the critical difference in the carrier-doping levels and CDW properties, must be properly taken into account to understand the microscopic mechanism behind the intriguing surface electronic anomalies in AV$_3$Sb$_5$.

In conclusion, the present micro-ARPES study of CsV$_3$Sb$_5$ has revealed the polar nature of the cleaved surface and self-doping effects. We uncovered that the Sb-terminated surface is characterized by excess hole doping and resultant suppression of CDW, whereas the Cs-terminated surface shows the band doubling and the resultant CDW-gap opening below T_{CDW} which support the 3D CDW. The present result opens a pathway toward understanding and manipulating exotic properties in kagome superconductors AV$_3$Sb$_5$.

[1] W. Shockley, Phys. Rev. **56**, 317 (1939).

[2] Y. A. Bychkov and E. I. Rashba, JETP Lett. **39**, 78 (1984).

[3] M. Z. Hasan and C. L. Kane, Rev. Mod. Phys. **82**, 3045 (2010).

[4] X.-L. Qi and S.-C. Zhang, Rev. Mod. Phys. **83**, 1057 (2011).

[5] Y. Ando, J. Phys. Soc. Jpn. **82**, 102001 (2013).

[6] A. Ohtomo and H. Y. Hwang, Nature (London) **427**, 423 (2004).

[7] A. D. Caviglia, S. Gariglio, N. Reyren, D. Jaccard, T. Schneider, M. Gabay, S. Thiel, G. Hammerl, J. Mannhart, and J.-M. Triscone, Nature (London) **456**, 624 (2008).

[8] S. Thiel, G. Hammerl, A. Schmehl, C. W. Schneider, and J. Mannhart, Science **313**, 1942 (2006).

[9] W. Meevasana, P. D. C. King, R. H. He, S.-K. Mo, M. Hashimoto, A. Tamai, P. Songsiriritthigul, F. Baumberger, and Z.-X. Shen, Nat. Mater. **10**, 114 (2011).

[10] A. F. Santander-Syro, O. Copie, T. Kondo, F. Fortuna, S. Pailhès, R. Weht, X. G. Qiu, F. Bertran, A. Nicolaou, A. Taleb-Ibrahimi, P. L. Fèvre, G. Herranz, M. Bibes, N. Reyren, Y. Apertet, P. Lecoeur, A. Barthélèmy, and M. J. Rozenberg, Nature (London) **469**, 189 (2011).

[11] H. Nakamura, T. Koga, and T. Kimura, Phys. Rev. Lett. **108**, 206601 (2012).

[12] S. McKeown Walker, A. de la Torre, F. Y. Bruno, A. Tamai, T. K. Kim, M. Hoesch, M. Shi, M. S. Bahramy, P. D. C. King, and F. Baumberger, Phys. Rev. Lett. **113**, 177601 (2014).

[13] K. Nakayama, T. Sato, K. Terashima, H. Matsui, T. Takahashi, M. Kubota, K. Ono, T. Nishizaki, Y. Takahashi, and N. Kobayashi, Phys. Rev. B **75**, 014513 (2007).

[14] V. B. Zabolotnyy, S. V. Borisenko, A. A. Kordyuk, J. Geck, D. S. Inosov, A. Koitzsch, J. Fink, M. Knupfer, B. Büchner, S.-L. Drechsler, H. Berger, A. Erb, M. Lambacher, L. Patthey, V. Hinkov, and B. Keimer, Phys. Rev. B **76**, 064519 (2007).

[15] F. Mazzola, V. Sunko, S. Khim, H. Rosner, P. Kushwaha, O. J. Clark, L. Bawden, I. Marković, T. K. Kim, M. Hoesch, A. P. Mackenzie, and P. D. C. King, Proc. Natl. Acad. Sci. USA **115**, 12956 (2018).

[16] K. Ishizaka, M. S. Bahramy, H. Murakawa, M. Sakano, T. Shimojima, T. Sonobe, K. Koizumi, S. Shin, H. Miyahara, A. Kimura, T. Okuda, H. Namatame, M. Taniguchi, R. Arita, N. Nagaosa, K. Kobayashi, Y. Murakami, R. Kumai, Y. Kaneko, Y. Onose *et al.*, Nat. Mater. **10**, 521 (2011).

[17] H. Maaß, H. Bentmann, C. Seibel, C. Tusche, S. V. Eremeev, T. R. F. Peixoto, O. E. Tereshchenko, K. A. Kokh, E. V. Chulkov, J. Kirschner, and F. Reinert, Nat. Commun. **7**, 11621 (2016).

[18] S. Souma, Z. Wang, H. Kotaka, T. Sato, K. Nakayama, Y. Tanaka, H. Kimizuka, T. Takahashi, K. Yamauchi, T. Oguchi, K. Segawa, and Y. Ando, Phys. Rev. B **93**, 161112(R) (2016).

[19] B. R. Ortiz, P. M. Sarte, E. M. Kenney, M. J. Graf, S. M. L. Teicher, R. Seshadri, and S. D. Wilson, Phys. Rev. Mater. **5**, 034801 (2021).

[20] B. R. Ortiz, S. M. L. Teicher, Y. Hu, J. L. Zuo, P. M. Sarte, E. C. Schueller, A. M. M. Abeykoon, M. J. Krogstad, S. Rosenkranz, R. Osborn, R. Seshadri, L. Balents, J. He, and S. D. Wilson, Phys. Rev. Lett. **125**, 247002 (2020).

[21] Q. Yin, Z. Tu, C. Gong, Y. Fu, S. Yan, and H. Lei, Chin. Phys. Lett. **38**, 037403 (2021).

[22] H. Chen, H. Yang, B. Hu, Z. Zhao, J. Yuan, Y. Xing, G. Qian, Z. Huang, G. Li, Y. Ye, S. Ma, S. Ni, H. Zhang, Y. Qiangwei, C. Gong, Z. Tu, H. Lei, H. Tan, S. Zhou, C. Shen *et al.*, Nature (London) **599**, 222 (2021).

[23] Y.-X. Jiang, J.-X. Yin, M. M. Denner, N. Shumiya, B. R. Ortiz, G. Xu, Z. Guguchia, J. He, M. S. Hossain, X. Liu, X. Liu, J. Ruff, L. Kautzsch, S. S. Zhang, G. Chang, I. Belopolski, Q. Zhang, T. A. Cochran, D. Multer, M. Litskevich *et al.*, Nature Mater. **20**, 1353 (2021).

[24] H. Zhao, H. Li, B. R. Ortiz, S. M. L. Teicher, T. Park, M. Ye, Z. Wang, L. Balents, S. D. Wilson, and I. Zeljkovic, Nature (London) **599**, 216 (2021).

[25] Z. Liang, X. Hou, F. Zhang, W. Ma, P. Wu, Z. Zhang, F. Yu, J.-J. Ying, K. Jiang, L. Shan, Z. Wang, and X.-H. Chen, Phys. Rev. X **11**, 031026 (2021).

[26] Z. Wang, Y.-X. Jiang, J.-X. Yin, Y. Li, G.-Y. Wang, H.-L. Huang, S. Shao, J. Liu, P. Zhu, N. Shumiya, M. S. Hossain, H. Liu, Y. Shi, J. Duan, X. Li, G. Chang, P. Dai, Z. Ye, G. Xu, Y. Wang *et al.*, Phys. Rev. B **104**, 075148 (2021).

[27] N. Shumiya, M. S. Hossain, J.-X. Yin, Y.-X. Jiang, B. R. Ortiz, H. Liu, Y. Shi, Q. Yin, H. Lei, S. S. Zhang, G. Chang, Q. Zhang, T. A. Cochran, D. Multer, M. Litskevich, Z.-J. Cheng, X. P. Yang, Z. Guguchia, S. D. Wilson, and M. Z. Hasan, Phys. Rev. B **104**, 035131 (2021).

[28] L. Nie, K. Sun, W. Ma, D. Song, L. Zheng, Z. Liang, P. Wu, F. Yu, J. Li, M. Shan, D. Zhao, S. Li, B. Kang, Z. Wu, Y. Zhou, K. Liu, Z. Xiang, J. Ying, Z. Wang, T. Wu *et al.*, Nature (London) **604**, 59 (2022).

[29] H. Li, Y.-X. Jiang, J. X. Yin, S. Yoon, A. R. Lupini, Y. Pai, C. Nelson, A. Said, Y. M. Yang, Q. W. Yin, C. S. Gong, Z. J. Tu, H. C. Lei, B. Yan, Z. Wang, M. Z. Hasan, H. N. Lee, and H. Miao, arXiv:2109.03418.

[30] H.-S. Xu, Y.-J. Yan, R. Yin, W. Xia, S. Fang, Z. Chen, Y. Li, W. Yang, Y. Guo, and D.-L. Feng, Phys. Rev. Lett. **127**, 187004 (2021).

[31] B. R. Ortiz, L. C. Gomes, J. R. Morey, M. Winiarski, M. Bordelon, J. S. Mangum, I. W. H. Oswald, J. A. Rodriguez-Rivera, J. R. Neilson, S. D. Wilson, E. Ertekin, T. M. McQueen, and E. S. Toberer, Phys. Rev. Mater. **3**, 094407 (2019).

[32] K. Nakayama, Y. Li, T. Kato, M. Liu, Z. Wang, T. Takahashi, Y. Yao, and T. Sato, Phys. Rev. B **104**, L161112 (2021).

[33] M. Kitamura, S. Souma, A. Honma, D. Wakabayashi, H. Tanaka, A. Toyoshima, K. Amemiya, T. Kawakami, K. Sugawara, K. Nakayama, K. Yoshimatsu, H. Kumigashira, T. Sato, and K. Horiba, Rev. Sci. Instrum. **93**, 033906 (2022).

[34] Y. Luo, S. Peng, S. M. L. Teicher, L. Huai, Y. Hu, B. R. Ortiz, Z. Wei, J. Shen, Z. Ou, B. Wang, Y. Miao, M. Guo, M. Shi, S. D. Wilson, and J.-F. He, arXiv:2106.01248.

[35] See Supplemental Material at http://link.aps.org/supplemental/10.1103/PhysRevB.106.L121112 for photoelectron emission angle dependence of core-level spectra, peak position of the Cs-4d core levels, surface-termination dependence of the saddle-point position, reproducibility of polar-surface formation, band splitting observed in the Cs-terminated surface, a signature of in-plane band folding, comparison of Fermi surface between Cs- and Sb-terminated surfaces, and comparison between the experimental and calculated band structures, which includes Refs. [25,32,38,40,49–51].

[36] K. Nakayama, Y. Li, T. Kato, M. Liu, Z. Wang, T. Takahashi, Y. Yao, and T. Sato, Phys. Rev. X **12**, 011001 (2022).

[37] C. Wang, S. Liu, H. Jeon, and J.-H. Cho, Phys. Rev. B **105**, 045135 (2022).

[38] H. Tan, Y. Liu, Z. Wang, and B. Yan, Phys. Rev. Lett. **127**, 046401 (2021).

[39] Y. Fu, N. Zhao, Z. Chen, Q. Yin, Z. Tu, C. Gong, C. Xi, X. Zhu, Y. Sun, K. Liu, and H. Lei, Phys. Rev. Lett. **127**, 207002 (2021).

[40] H. Li, T. T. Zhang, T. Yilmaz, Y. Y. Pai, C. E. Marvinney, A. Said, Q. W. Yin, C. S. Gong, Z. J. Tu, E. Vescovo, C. S. Nelson, R. G. Moore, S. Murakami, H. C. Lei, H. N. Lee, B. J. Lawrie, and H. Miao, Phys. Rev. X **11**, 031050 (2021).

[41] R. Lou, A. Fedorov, Q. Yin, A. Kuibarov, Z. Tu, C. Gong, E. F. Schwier, B. Büchner, H. Lei, and S. Borisenko, Phys. Rev. Lett. **128**, 036402 (2022).

[42] Z. Liu, N. Zhao, Q. Yin, C. Gong, Z. Tu, M. Li, W. Song, Z. Liu, D. Shen, Y. Huang, K. Liu, H. Lei, and S. Wang, Phys. Rev. X **11**, 041010 (2021).

[43] S. Cho, H. Ma, W. Xia, Y. Yang, Z. Liu, Z. Huang, Z. Jiang, X. Lu, J. Liu, Z. Liu, J. Li, J. Wang, Y. Liu, J. Jia, Y. Guo, J. Liu, and D. Shen, Phys. Rev. Lett. **127**, 236401 (2021).

[44] H. Luo, Q. Gao, H. Liu, Y. Gu, D. Wu, C. Yi, J. Jia, S. Wu, X. Luo, Y. Xu, L. Zhao, Q. Wang, H. Mao, G. Liu, Z. Zhu, Y. Shi, K. Jiang, J. Hu, Z. Xu, and X. J. Zhou, Nat. Commun. **13**, 273 (2022).

[45] M. Kang, S. Fang, J.-K. Kim, B. R. Ortiz, S. H. Ryu, J. Kim, J. Yoo, G. Sangiovanni, D. Di Sante, B.-G. Park, C. Jozwiak, A. Bostwick, E. Rotenberg, E. Kaxiras, S. D. Wilson, J.-H. Park, and R. Comin, Nat. Phys. **18**, 301 (2022).

[46] T. Kato, Y. Li, T. Kawakami, M. Liu, K. Nakayama, Z. Wang, A. Moriya, K. Tanaka, T. Takahashi, Y. Yao, and T. Sato, Commun. Mater. **3**, 30 (2022).

[47] Y. Hu, X. Wu, B. R. Ortiz, S. Ju, X. Han, J. Ma, N. C. Plumb, M. Radovic, R. Thomale, S. D. Wilson, A. P. Schnyder, and M. Shi, Nat. Commun. **13**, 2220 (2022).

[48] Y. Cai, Y. Wang, Z. Hao, Y. Liu, X.-M. Ma, Z. Shen, Z. Jiang, Y. Yang, W. Liu, Q. Jiang, Z. Liu, M. Ye, D. Shen, Z. Sun, J. Chen, L. Wang, C. Liu, J. Lin, J. Wang, B. Huang *et al.*, arXiv:2109.12778.

[49] G. Pirug, A. Winkler, and H. P. Bonzel, Surf. Sci. **163**, 153 (1985).

[50] P. Zhang, P. Richard, N. Xu, Y.-M. Xu, J. Ma, T. Qian, A. V. Fedorov, J. D. Denlinger, G. D. Gu, and H. Ding, Appl. Phys. Lett. **105**, 172601 (2014).

[51] B. R. Ortiz, S. M. L. Teicher, L. Kautzsch, P. M. Sarte, N. Ratcliff, J. Harter, J. P. C. Ruff, R. Seshadri, and S. D. Wilson, Phys. Rev. X **11**, 041030 (2021).